Supporting Information

A fiber-shaped ultrasonic transducer by designing flexible epoxy/nano-zirconia composite as acoustic matching layer

Jiaqi Wu[†], Yichi Zhang[†], Yue Liu, Yuanyuan Zheng, Kailiang Xu*, Peining Chen*, Huisheng Peng

J. Wu, Y. Zhang, Y. Liu, Y. Zheng, Prof. P. Chen, Prof. H. Peng
[a] State Key Laboratory of Molecular Engineering of Polymers, Department of Macromolecular Science, Institute of Fiber Materials and Devices, Laboratory of Advanced Materials, Fudan University, Shanghai 200438, China, E-mail: peiningc@fudan.edu.cn.

Prof. K. Xu
[b] Department of Biomedical Engineering, State Key Laboratory of Integrated Chips and Systems, Fudan University, Shanghai 200438, China; Shanghai Poda Medical Technology Co., Ltd., Shanghai, China，E-mail: xukl@fudan.edu.cn.

[†]The first two authors contributed equally to this work.

Supporting Note 1: Experimental details

(1) Spin-coating processes and parameters of epoxy/nano-zirconia composite.

The silicon wafer was treated with surface oxygen plasma and then the intradex solution (5 wt%, Aladdin) was added onto the silicon wafer to spin coat. The spin-coating rate was 3000 rpm (round per minute) and the time was 10 s. Bake the silicon wafer to remove water from the intradex solution to form a sacrificing layer. The epoxy/nano-zirconia composite could be spin-coated on the sacrificing layer. The specific spin-coating rate is shown in Supplementary Figure 6d, and the time was 30 s. Repeat the spin-coating process several times after curing of composite to obtain the epoxy/nano-zirconia composite with specific thickness.

(2) Deposition of conductive path.

The patterned tungsten mask was obtained by laser engraving. The metal film layers were deposited through the patterned tungsten mask on the flexible composite matching layer by magnetron sputtering or thermal evaporation. The conductive path obtained is shown in Supplementary Figure 8. The shape and material of the conductive path and the thickness of metal film layer are determined according to the experimental requirements.

(3) Preparation and connection of piezoelectric elements.

The piezoelectric elements (1-3 piezoelectric composite, Innovia Materials (Shanghai) Co., Ltd) were cut into 900 μm × 900 μm × 350 μm blocks by diamond wire cutting machine. The piezoelectric elements were bonded with conductive path on the flexible composite matching layer by conductive silver adhesives.

(4) Encapsulation and cutting of fiber-shaped ultrasonic transducers.

Highly transparent flexible epoxy resin (3016, Hasuncast) was injected into the gap between two flexible composite matching layers and cured at room temperature to obtain the ultrasonic transducer array. The fiber-shaped ultrasonic transducers were further obtained by cutting the ultrasonic transducer array with a diamond wire cutting machine.

Supporting Note 2: The characteristics of the acoustic matching layer for ultrasonic transducer

To understand the characteristics of the acoustic matching layer for ultrasonic transducers, it is necessary to understand the acoustic impedance of material and the reflection and transmission of sound waves between different media.

The acoustic impedance Z can be expressed as:

$$Z = \rho \times c \tag{2-1}$$

Where, ρ is the density of the material, and c is the sound velocity of material.

Due to the difference in acoustic impedance of different acoustic propagation media, when sound waves propagate from one medium to another, the reflection and transmission of sound waves will be generated at the interface of the two media. The transmittance T can be expressed as:

$$T = \frac{4Z_1Z_2}{(Z_1 + Z_2)^2} \tag{2-2}$$

Where, Z_1 and Z_2 are the acoustic impedances of different media, respectively.

The acoustic impedances of piezoelectric elements and human tissue differ greatly, resulting in low ultrasonic transmittance. When an acoustic matching layer is added between the piezoelectric element and the human tissue, the reflection and transmission will be greatly changed. If the thickness of the matching layer is $(2N + 1)\lambda/4$ (Where λ is the wavelength of ultrasound, N is a natural number), the acoustic intensity transmittance T_{PL} between the piezoelectric element and human tissue can be expressed as:

$$T_{PL} = \frac{4Z_PZ_L}{(Z_M + \frac{Z_P + Z_L}{Z_M})^2} \tag{2-3}$$

Where Z_P, Z_L and Z_M are the acoustic impedance of piezoelectric element, human tissue, and matching layer, respectively.

The ideal acoustic impedance Z_M can be expressed as:

$$Z_M = \sqrt{Z_P Z_L} \tag{2-4}$$

When the acoustic impedance of the matching layer reaches the ideal value and the thickness is $(2N + 1)\,\lambda/4$, the ultrasonic wave generated by the piezoelectric element can be almost all transmitted into the external medium to achieve the ideal acoustic matching. Of course, there will be other factors in the actual experiment. For minimizing the impact of acoustic attenuation, it is most appropriate to select a quarter wavelength for the thickness of the matching layer. The acoustic impedance of human tissue and 1-3 piezoelectric composite are 1.5 MRayl and 17.1 MRayl respectively, so the ideal acoustic impedance of matching layer for them is about 5.1 MRayl.

The wavelength of ultrasound λ can be calculated by:

$$\lambda = c/f \tag{2-5}$$

Where c is the sound velocity in material, f is the frequency of ultrasound. The sound velocity can be measured by the principle showed in Supplementary Figure 3. The sound velocity in epoxy/nano-zirconia composite was 2330 m/s and the designed frequency was 5 MHz, so the wavelength of ultrasound in composite (calculated by Formula 2-5) was 466 μm and the ideal thickness of matching layer was 116.5 μm.

Supporting Note 3: The principle of monitoring blood pressure by ultrasonic transducer

After the ultrasonic wave enters the human body, it is reflected when it meets the anterior and posterior walls of artery respectively. According to the time difference of the reflected wave received by ultrasonic transducer, the artery diameter $d(t)$ can be calculated:

$$d(t) = \frac{t_2 - t_1}{2} v$$

(3-1)

Where t_1 is the time of reflected wave front anterior wall of artery, t_2 is the time of reflected wave front posterior wall of artery, and v is the average sound velocity in human body.

Relevant studies have shown that there is a relationship between blood pressure and the cross-sectional area of artery. Therefore, the waveform of blood pressure can be calculated according to the waveform change of artery diameter. The cross section of artery can be approximately circular, and the cross-sectional area $A(t)$ can be expressed as:

$$A(t) = \frac{\Pi d^2(t)}{4}$$

(3-2)

The waveform of blood pressure can be expressed as:

$$P（t） = P_d \times exp\{\alpha \times f（t）\}$$

(3-3)

Where P_d is the diastolic blood pressure of artery, α is the stiffness coefficient of artery, which is a constant. The dilation coefficient of artery $f（t）$ can be expressed as:

$$f（t） = \frac{A（t）}{A_d} - 1$$

(3-4)

Where A_d is the cross-sectional area of artery during diastole.

In addition, the stiffness coefficient of artery can be corrected with the following formula to obtain a more accurate waveform of blood pressure:

$$\alpha = \frac{A_d ln\left(\frac{P_s}{P_d}\right)}{A_s - A_d}$$

Where A_s is the cross-sectional area of artery during systole, and P_s is the systolic blood pressure of the artery.

The systolic and diastolic blood pressure of artery can be measured by commercial blood pressure monitoring devices.

Table S1. Sound velocity, density, and acoustic impedance of typical functional polymers

Material	Sound velocity (m/s)	Density (g/cm³)	Acoustic impedance (MRayl)	Supplier and model
PVDF	2150	1.82	3.91	Sigma-Aldrich, 182702
PET	2298	1.36	3.12	Billion Industrial Holding Co., Ltd, CAN21-062480
PE	1900	0.96	1.82	Sigma-Aldrich, S428078
PI	2200	1.42	3.12	Dupont, Vespel-SP1
PDMS	1030	1.01	1.04	Dow corning, Sylgard 184
TPU	1860	1.24	2.31	BASF, 85AHT
EP	2600	1.18	3.06	Yi Tuo Composite Material (Kun Shan) Co., Ltd, E51
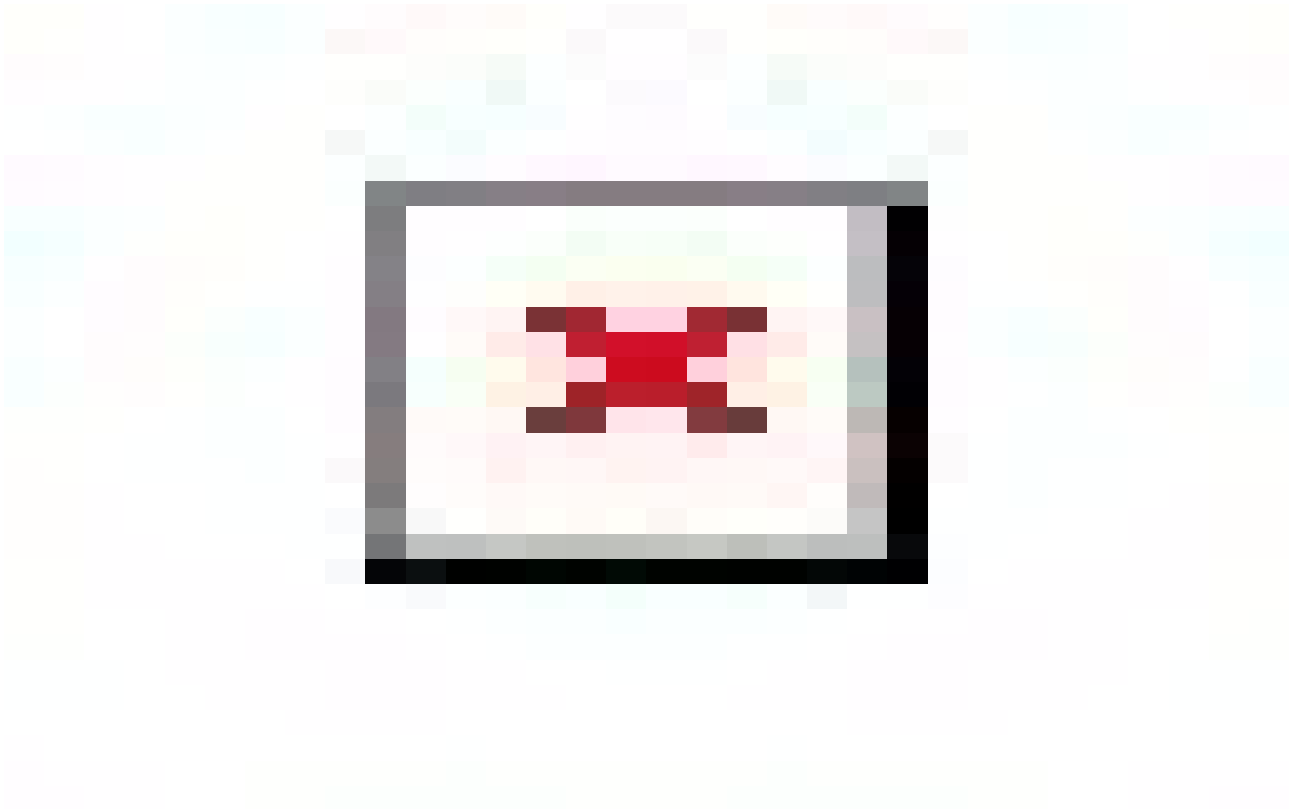
Fig. S1. Schematic diagram of preparation process of EP/ZrO$_2$ composite.
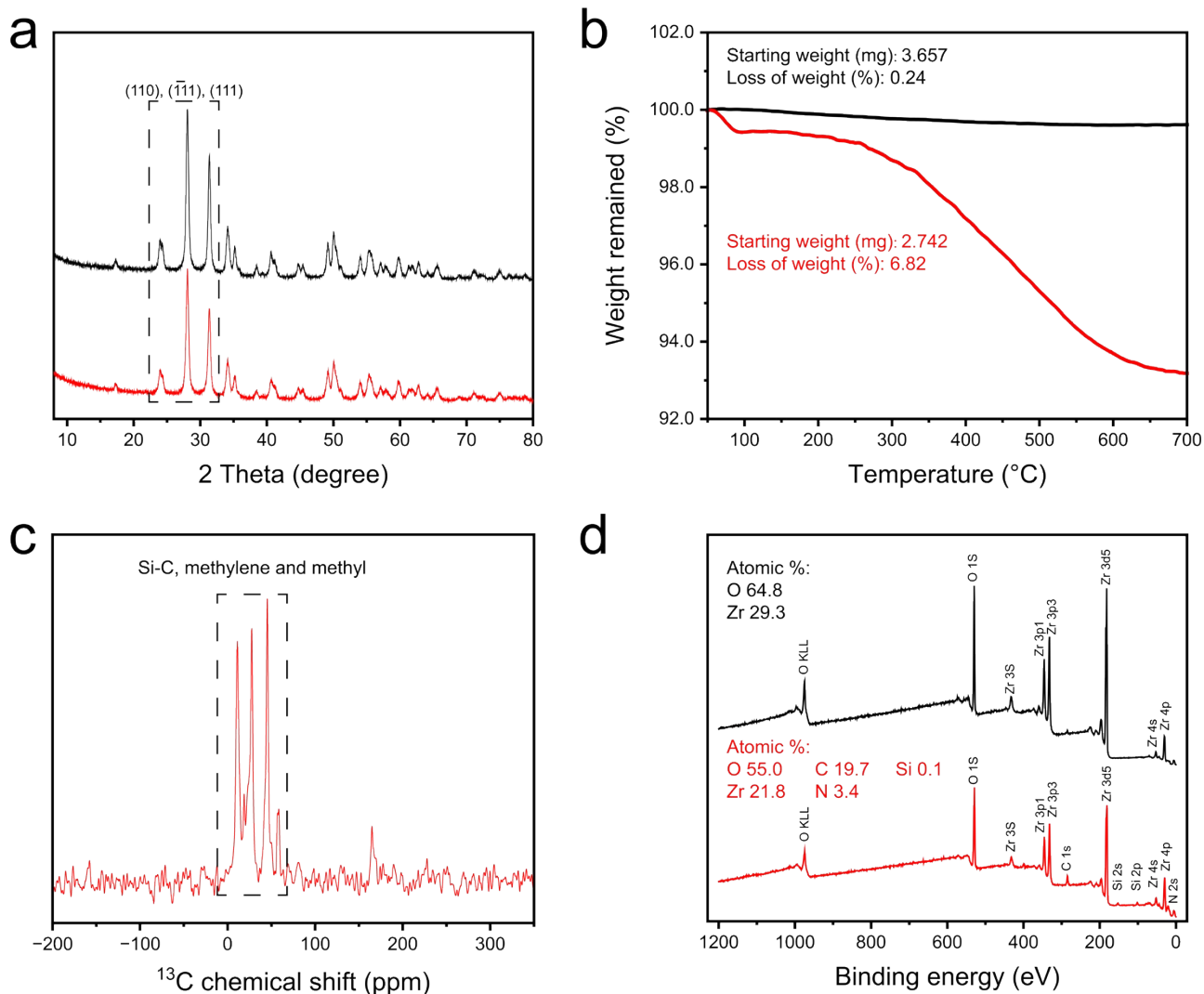
Fig. S2. (a) XRD spectra of nano-zirconia particles before and after modification. (b) TGA curves of nano-zirconia particles before (black line) and after modification (red line). (c) ^{13}C NMR spectra of nano-zirconia particles after modification. (d) XPS spectra of nano-zirconia particles before (black line) and after modification (red line).
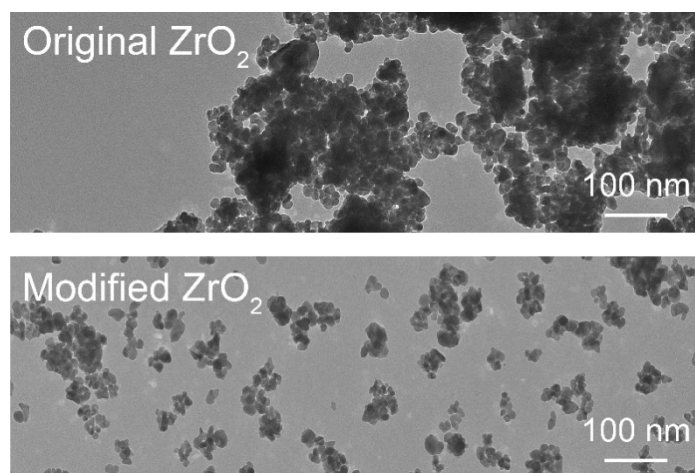
Fig. S3. TEM images of original and modified nano-zirconia particles.
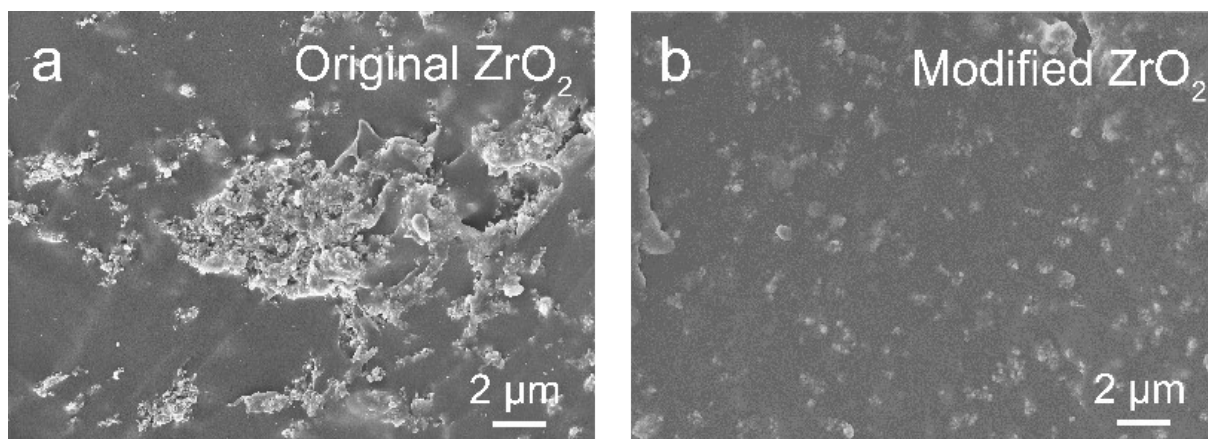
Fig. S4. SEM images of original (a) and modified nano-zirconia particles (b) in the composite.
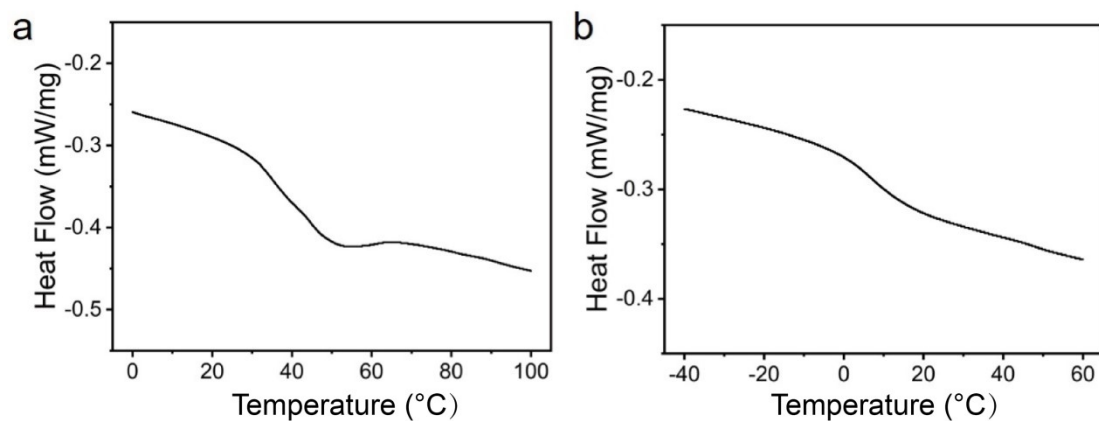
Fig. S5. Differential scanning calorimetry of pure epoxy resin (a) and epoxy/nano-zirconia composite (b). The glass-transition temperature of pure epoxy resin was over 40 °C, which was in a glassy state, but the glass-transition temperature of epoxy/nano-zirconia composite was about 10 °C, which was in a high-elastic state.
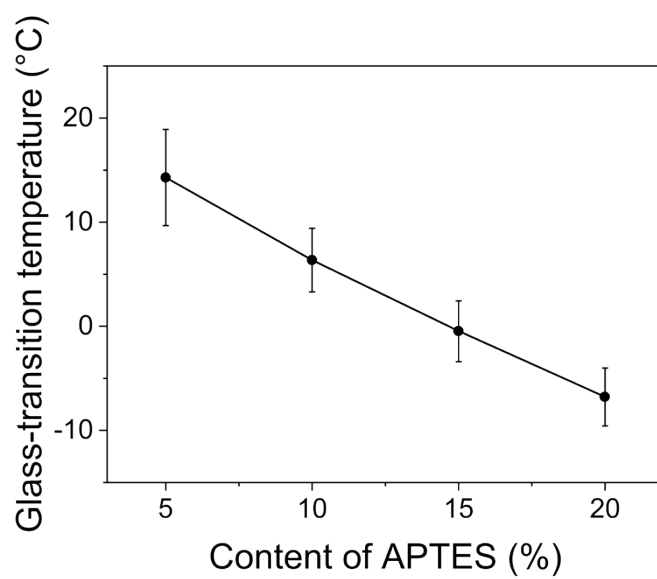
Fig. S6. The glass-transition temperature of epoxy/nano-zirconia composite along with different content of APTES.
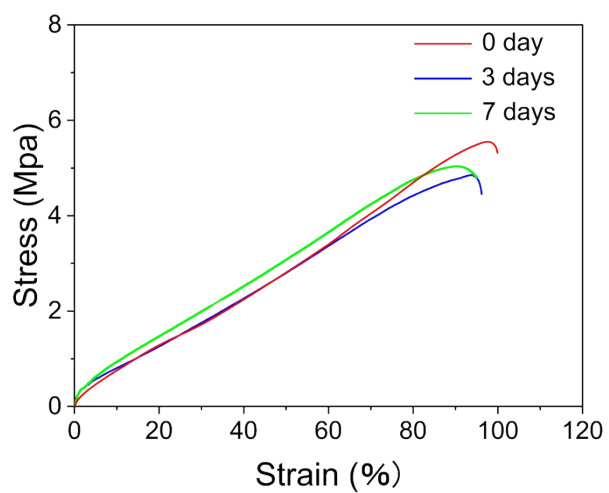
Fig. S7. Comparison of stress-strain curves of of EP/ZrO$_2$ composite after long-term storage under room temperature conditions.
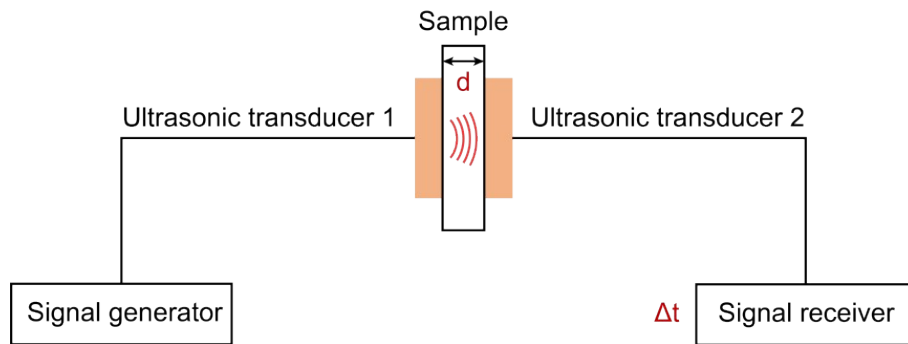
Fig. S8. Schematic diagram of the principle of sound velocity measurement. Two ultrasonic transducers are used to connect signal generator and signal receiver. The sample with a certain thickness d is placed between two transducers. The ultrasonic transducer No.1 transmits ultrasonic signals through the sample, and the ultrasonic signals are received by ultrasonic transducer No.2. The time interval (Δt) between transmission and reception can be calculated. The sound velocity c in the sample can be calculated by formula $c = d/\Delta t$, and the sound attenuation coefficient can be expressed by formula $\alpha = 0.107 f Z/V$, where f is the ultrasonic frequency, Z is the acoustic impedance, and V is the velocity of sound in the medium.
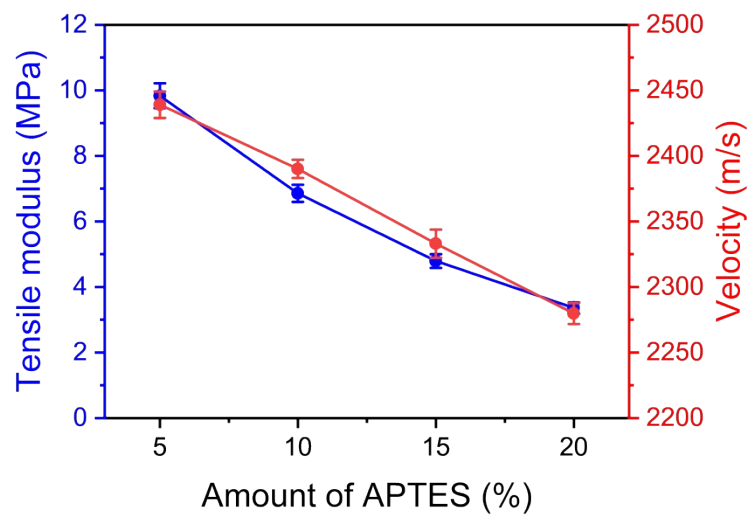
Fig. S9. The modulus and sound velocity of epoxy/nano-zirconia composite with different amounts of APTES.
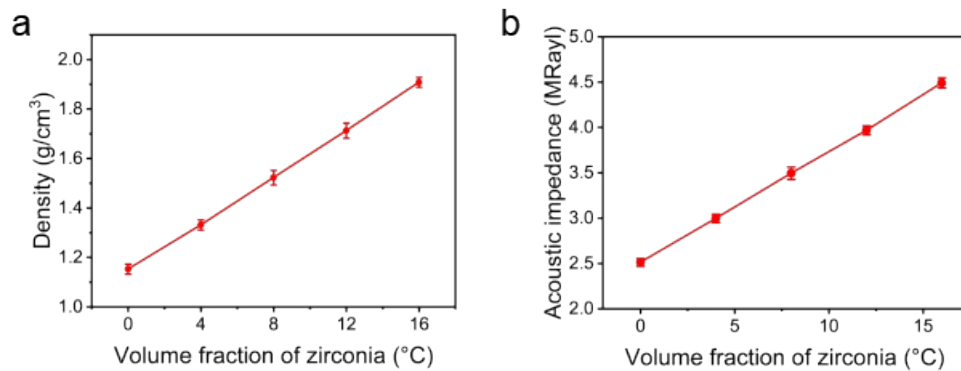
Fig. S10. The density (a) and acoustic impedance (b) of epoxy/nano-zirconia composite with different volume fraction of nano-zirconia.
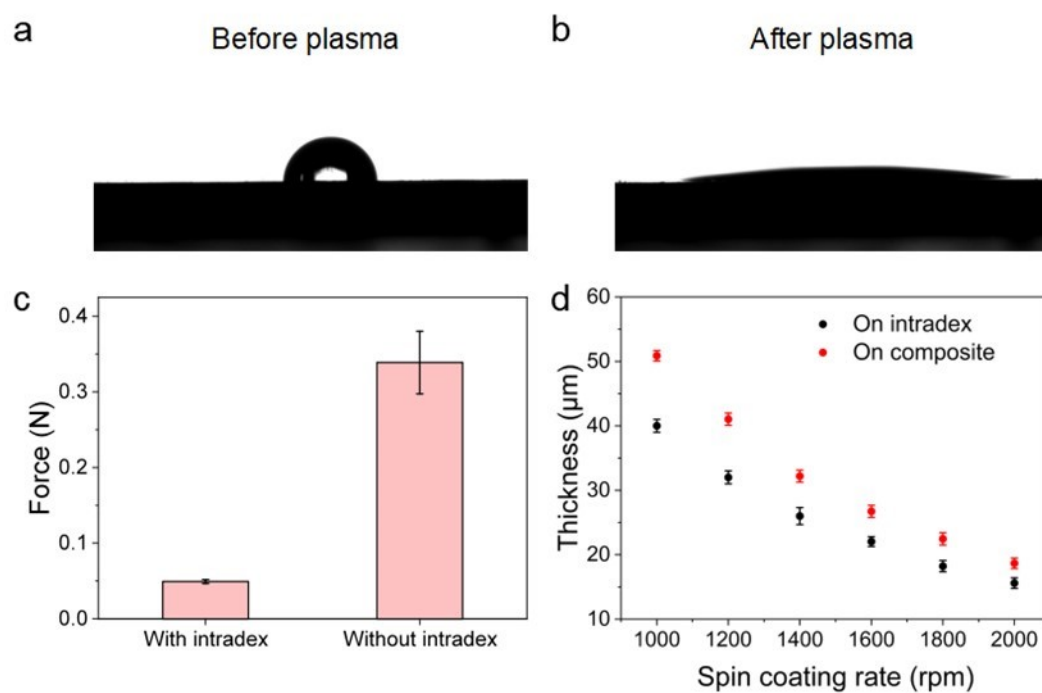
Fig. S11. Comparison of the contact angle of the silicon wafer surface before plasma treatment (a) and after plasma treatment (b). (c) The stripping force of the silicon wafer surface with or without sacrificing layer. (d) Differences in spin-coating parameters between intradex and composite surfaces
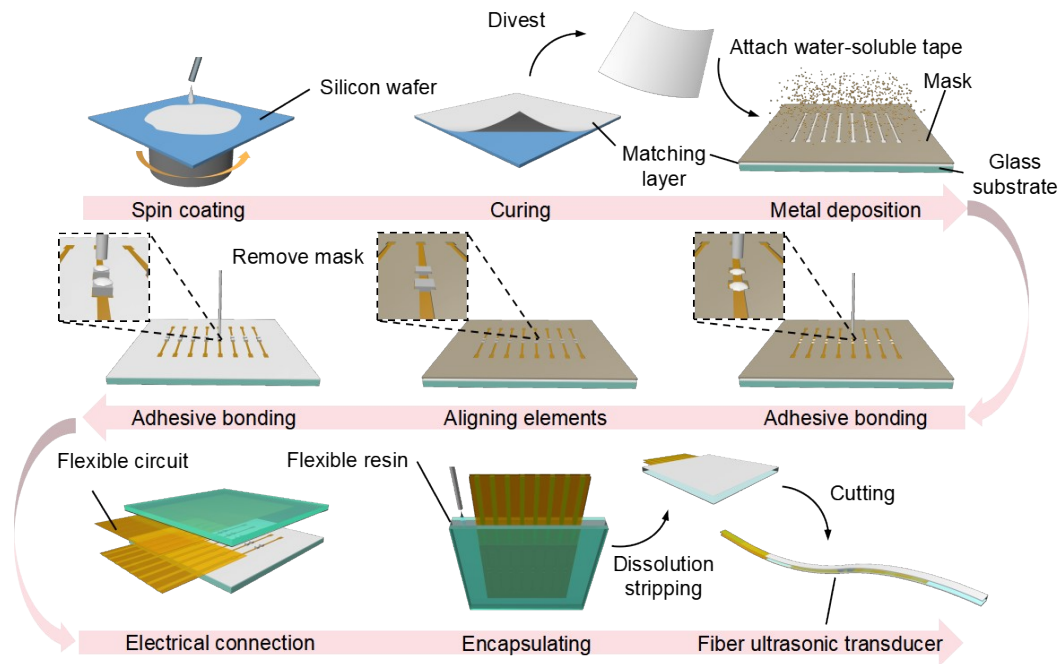
Fig. S12. Schematic diagram of fabrication process of fiber-shaped ultrasonic transducer.
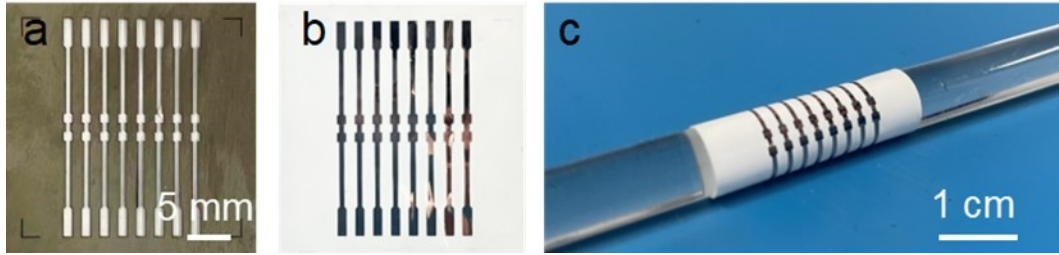
Fig. S13. (a) Patterned tungsten mask for depositing conductive paths. (b) The photo of flexible composite matching layer after depositing conductive path. (c) Display of deformability of flexible composite matching layer after deposition conductive path.
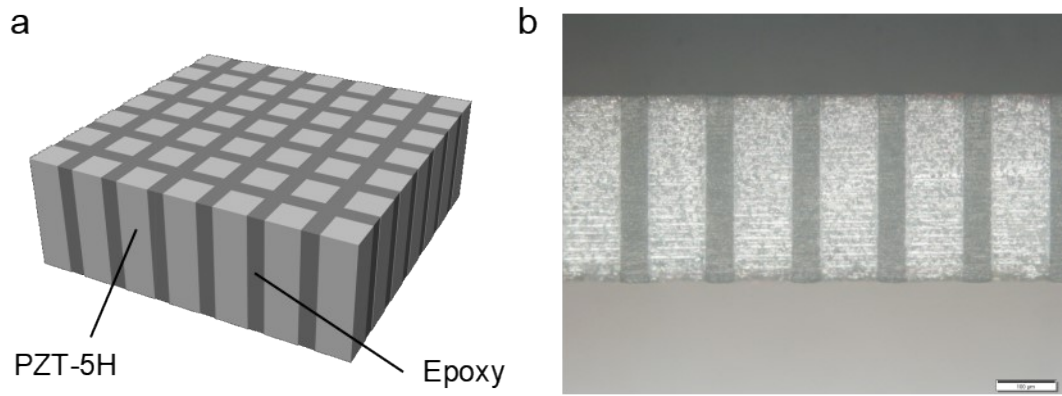
Fig. S14. (a) Schematic diagram of 1-3 composite structure, which is consisted of PZT-5H pillars and epoxy resin. (b) The photograph of 1-3 composite under the optical microscope, where the width of PZT-5H pillars and the epoxy resin is 100 μm and 50 μm, respectively.
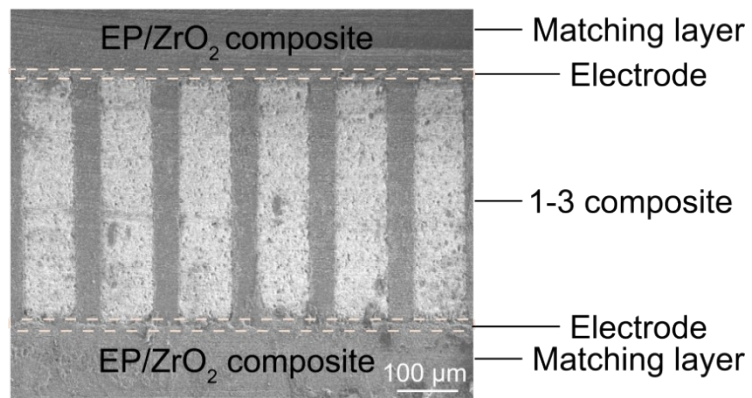
Fig. S15. Cross-sectional SEM image of fiber-shaped ultrasonic transducer.
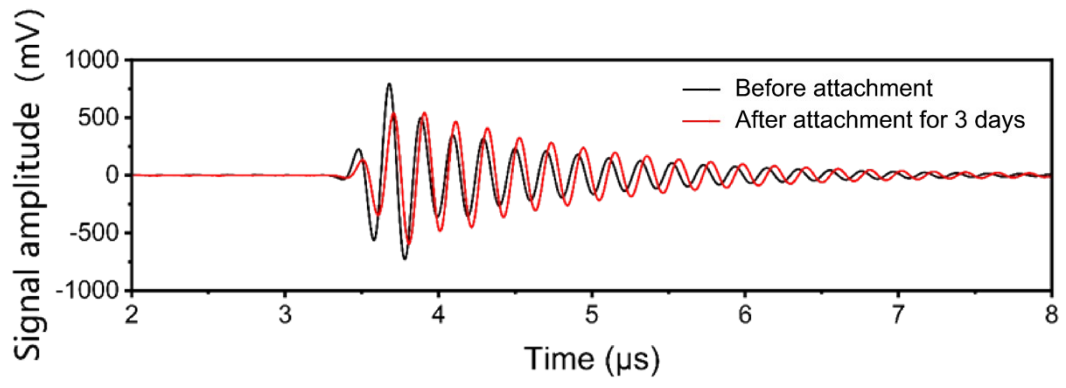
Fig. S16. Comparison of the operating signals of the ultrasound transducer before and after attachment to the mouse skin.
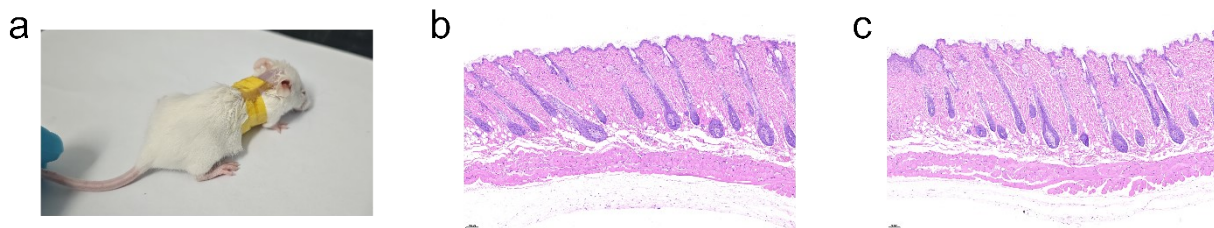
Fig. S17. (a) Photograph of the EP/ZrO$_2$ composite film being attached on the mouse skin. (b, c) Photographs of H&E staining of skin tissue before (a) and after (b) attaching of EP/ZrO$_2$ composite film on the mouse skin.